ISSN 1063-7729, Astronomy Reports, 2009, Vol. 53, No. 4, pp. 343–354. © Pleiades Publishing, Ltd., 2009.
Original Russian Text © M.M. Katsova, I.M. Livshits, J. Sykora, 2009, published in Astronomicheskiĭ Zhurnal, 2009, Vol. 86, No. 4, pp. 379–391.

The Rotation of the Sun as a Star from the Integrated Coronal Green-Line Emission

M. M. Katsova[1], I. M. Livshits[2], and J. Sykora[3]

[1]*Sternberg Astronomical Institute, Universitetskii pr. 13, Moscow, 119899, Russia*

[2]*Pushkov Institute of Terrestrial Magnetism, Ionosphere and Radio Wave Propagation, IZMIRAN, Troitsk, Moscow Region, 142190, Russia*

[3]*Institute of Astronomy, Slovak Academy of Sciences, Tatranska Lomnica, Slovakia*

Received 2008; in final form, July 2, 2008

Abstract—A new representation for the database collected by J. Sykora on the Fe XIV 5303 Å line emission observed from 1939 to 2001 is proposed. Observations of the corona at an altitude of 60″ above the limb reduced to a single photometric scale provide estimates of the emission of the entire visible solar surface. It is proposed to use the resulting series of daily measurements as a new index of the solar activity, GLSun (The Green-Line Sun). This index is purely observational and is free of the model-dependent limitations imposed on other indices of coronal activity. GLSun describes well both the cyclic activity and the rotational modulation of the brightness of the corona of the Sun as a star. The GLSun series was subject to a wavelet analysis similar to that applied to long-term variations in the chromospheric emission of late active stars. The brightness irregularities in the solar corona rotate more slowly during epochs of high activity than their average rotational speed over the entire observational interval. The interval of slower rotation of the irregularities is close to the epoch when the Sun's field represents a horizontal magnetic dipole in each activity cycle, but is somewhat longer than the duration of the polarity reversal in both hemispheres. The difference between the periods for the slower and mean rotation exceeds three days, as is typical for some stars with higher but more irregular activity than the Sun. The importance of these findings for dynamo theory for the origin and evolution of the magnetic fields of the Sun and other late-type stars is briefly discussed.

PACS numbers: 96.60.P-, 96.60.Bn
DOI: 10.1134/S1063772909040076

1. INTRODUCTION

The activity of late-type stars, including the Sun, is related to magnetic fields on various scales observed in the stellar atmospheres. The dynamo theory provides the most comprehensive models for the generation and enhancement of cosmic magnetic fields. This theory is based on the possiblity of amplfying magnetic fields via turbulent convection in a convective zone with differential rotation. Only the surface layers of the solar rotation have been studied so far. In recent years, information about the rotation of both the atmosphere and the entire convective zone has become available through helioseismology data. The angular velocity of the rotation increases from the base of the convective zone to its upper layers at low and middle latitudes, with the gradient $d\Omega/dr$ changing its sign at high latitudes [1]. The helioseismology data definitely support general ideas about the generation of magnetic fields, and stimulates deeper studies of the differential rotation of solar layers. The validity of the main concepts of the dynamo theory provide a basis for comparing the theory with observations, in particular those on the cyclicity of the Sun.

There are numerous long-living solar formations that enable us to examine the rotation of the Sun. The tracer method has been used for 150 yrs (Carrington's first work dates to 1858); the clearest results are obtained from the rotational velocities of sunspots, faculae, and prominences observed in zones of activity. Below latitudes of 60°, the rotation traced by active elements agrees well with spectroscopic measurements indicating the solar rotation via the Doppler shifts of spectral lines. Among numerous publications in this area, we note the review [2], which summarizes work carried out up to the end of the 20th century. Among recent works, we note those indicating that regions with a specified rotation change their latitudes during the solar cycle [3].

A detailed study of the coronal rotation over the several last cycles is presented in [4] (see also references therein), which considers data on the brightness of the Fe XIV 5303 Å coronal green line. Fig-

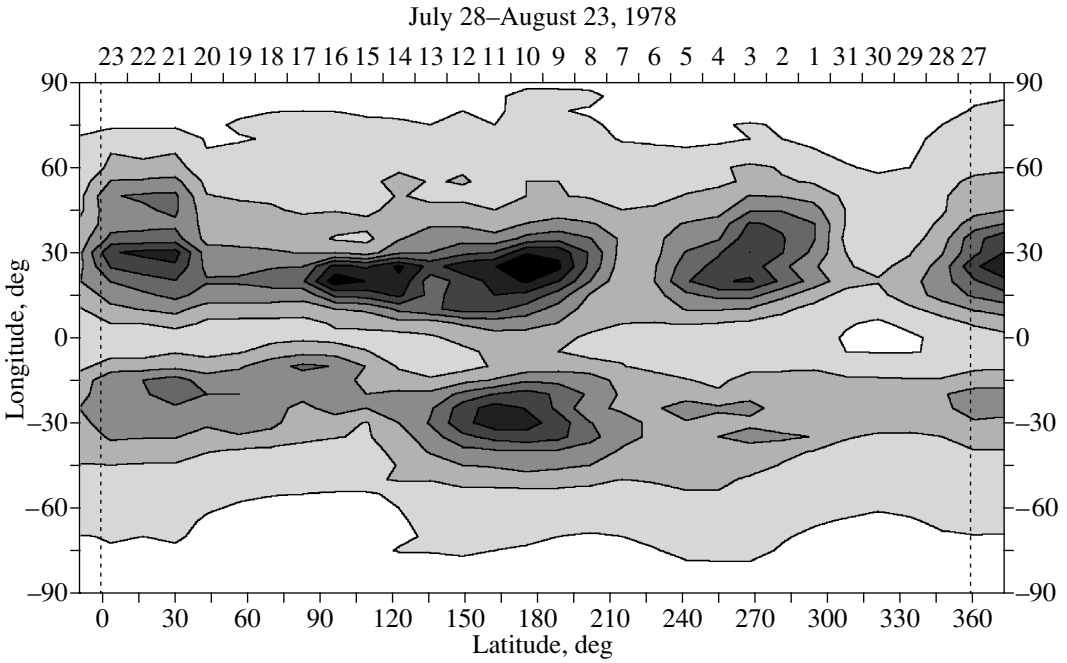

Fig. 1. Map of the coronal green-line brightness constructed from the database collected by J. Sykora in absolute coronal units (a.c.u.). The total range of brightnesses is divided in eight intervals, with the brightest shown as black and the weakest as white. The contour interval is 15 a.c.u. The upper horizontal axis shows time growing from right to left. Carrington rotation 1671 is shown dotted. The GLSun index for August 10, 1978 was calculated from this map.

ure 1 presents one of the maps used to make the film [5]. In [4], the rotation at various solar latitudes was determined from data averaged over six Carrington rotations. Among the main findings of [4] is that differential rotation occurs during the entire growth phase of the solar activity, while the rotation is close to rigid-body in the middle of the decay phase.

Studying the rotation of stars is a challenging astrophysical problem. As a rule, observations can be used to determine the rotational velocity, but attempts to estimate the degree of differential rotation give contradictory results. This is especially true for single stars, and is true to a lesser extent for binary stars, for which Doppler maps provide more or less reliable results. Therefore, there is substantial interest in new approaches to analyzing the rotation of late-type stars.

Studies of stars displaying solar-type activity indicate that some stars display rotations of their chromospheric irregularities that are slower than the mean rotations during several years [6]. In general, this can be explained by a scenario in which the active regions are located at middle latitudes during some phases of the cycles, with these regions drifting toward the equator. It is most natural to explain this drift as an effect of differential rotation. This enables the construction of stellar butterfly diagrams resembling the Maunder diagrams for the Sun.

It is very important to compare the results of [6] with those for the differential rotation of the Sun. This can be done using the results for the solar corona presented in [4]. Indeed, brightness irregularities related to the evolution of magnetic fields behave similarly at the chromospheric and coronal levels, and demonstrate a distinct cyclicity in the absence of powerful non-stationary processes. There is a uniform data series for the solar corona encompassing several solar cycles. In the first stage of this work, we directly compare results for the differential solar rotation with data on the rotation of other stars. However, the analysis of solar observations presented in [4] examines correlations corresponding to all longitudes within a given latitude interval. In addition, this analysis uses data averaged over six Carrington rotations. This approach underestimates the role of individual bright elements that contribue appreciably to the emission of the Sun as a star (compared to the emission of other stars). Consequently, a comparison of the results obtained in [4, 7] with the rotations of stars derived from daily observations is not quite correct, and leads to slight differences in the rotational periods of the Sun as a star determined during different phases of the solar cycle.

Since analyses of the solar and stellar rotations are carried out using different methods, a direct comparison of results becomes almost impossible. The present work proposes another approach, namely, we

first estimate the coronal emission of the Sun as a star and then apply a wavelet analysis to the time series obtained. Using a single method to analyze the long-term variability in the emission of the Sun and other late-type stars provides an adequate comparison of the rotational variability determined over several activity cycles for the Sun and other late-type stars. There are no reliable data on the magnetic fields on various scales for late-type stars, and heliophysical data are very helpful for interpreting stellar observations.

Below, we introduce a new index of the solar activity, obtain a wavelet transform for the daily data, and discuss our analysis of the solar rotation. We then briefly compare the differential rotation displayed by the Sun and by other active late-type stars.

2. ESTIMATES OF THE CORONAL BRIGHTNESS OF THE SUN AS A STAR

Monitoring coronal observations are carried out using Lyot coronographs at several observatories. The measurements slightly differ in the altitudes of the observed regions above the limb and he photometric scales used. J. Sykora has reduced the daily measurements of the Fe XIV 5303 Å coronal green line to a single photometric scale and an altitude of 60″ above the limb. The daily measurements on the eastern (E) and western (W) limbs carried out for every 5° of latitude were recalculated to the central meridian. Every brightness measurement derived for 1939–2001 is the half-sum of the brightnesses observed at the given latitude seven days before and seven days after the corresponding date. Thus, this corresponds to a database with a resolution of 5° in latitude and 13° in longitude. The array contains interpolated data for the 10%–15% of days with no observations. Every day in the database is represented by a column containing 17 brightness measurements in units of 10^{-6} of the intensity of the continuum near the line. To reduce the scatter in the data, each brightness in the final database is a sliding average carried out over three days.

These data can be used to calculate the total emission of the solar corona for each day of observations, if we assume that the conditions in the corona remain constant during the period when the source is observed on the visible hemisphere. However, we must take into account the geometry, structural features, and physical conditions as a funaction of the altitude of the radiation source.

The total coronal green-line emission was first calculated in [8], then in [9] and other works. The total coronal emission for a given day was determined as the visible line emission detected above the limb and the corresponding emission of the corona projected onto the visible solar disk. The flux of soft X-rays emitted from the same volume of the corona (the limb and disk) is an obvious analog. Starting from 1971, heliophysical studies have employed the coronal index introduced by M. Rybansky (see [10] for details).

X-ray observations of the Sun have shown that this index inadequately describes the long-term variability in the emission of coronal layers with temperatures of about 2 MK, which are responsible for the green-line emission. A technique used to calculate this index starting with [8] employs the mean brightness for a given day (see expression (3) in [8]) and interpolates the intensity from the altitude of observations downward to unperturbed and active regions. The accumulated information on the solar corona make it possible to introduce a clearer index that takes into account the contributions of both active regions and of regions located above the neutral line of the large-scale magnetic field to the total coronal emission of the Sun as a star.

Instead of using models for the source of the green-line emission, we propose to use the observational parameters directly, and introduce a new index that is approximately proportional to the integrated brightness of the corona detected at a specified altitude above the limb. The data for the coronal brightness detected over 27 successive days can be considered a Carrington map; an example is presented in. Fig. 1. We use the brightness $B(\varphi_n)$ for the chosen day (August 10, 1978 in Fig. 1), as well as seven days before and seven days after this day. In this case, to first approximation, the disk brightness per cell takes the form

$$\begin{aligned}\mathrm{GLSun} &= \sum\sum B(\varphi_n)\cos\varphi_n\cos\lambda_m \\ &= \sum\sum B(5^\circ n)\cos(5^\circ n)\cos(13^\circ m),\end{aligned}$$

where $B(\varphi_n)$ is the coronal brightness and n varies from $+14$ to -14 and m from $+7$ to -7. In other words, we assume that the regions located below 70° latitude provide the main brightness contribution and approximately take into account the change in a projected area covering 5° in latitude and 13° in longitude as a function of its coordinates on a sphere.

Figure 2b presents the results of our GLSun calculations. The cyclic activity seen here resembles that detected using other indices, such as the monthly averaged Wolf numbers. In terms of its physical meaning, GLSun is most similar to the X-ray background (the X-ray flux with flares eliminated) and the 10.7 cm radio emission. The X-ray background has been considered only infrequently in recent years, since it is difficult to eliminate flares, especially during periods of high activity. Similarly to the 10.7 cm radio emission, the GLSun coronal index is less sensitive to nonstationary processes (flares) than is the soft X-ray

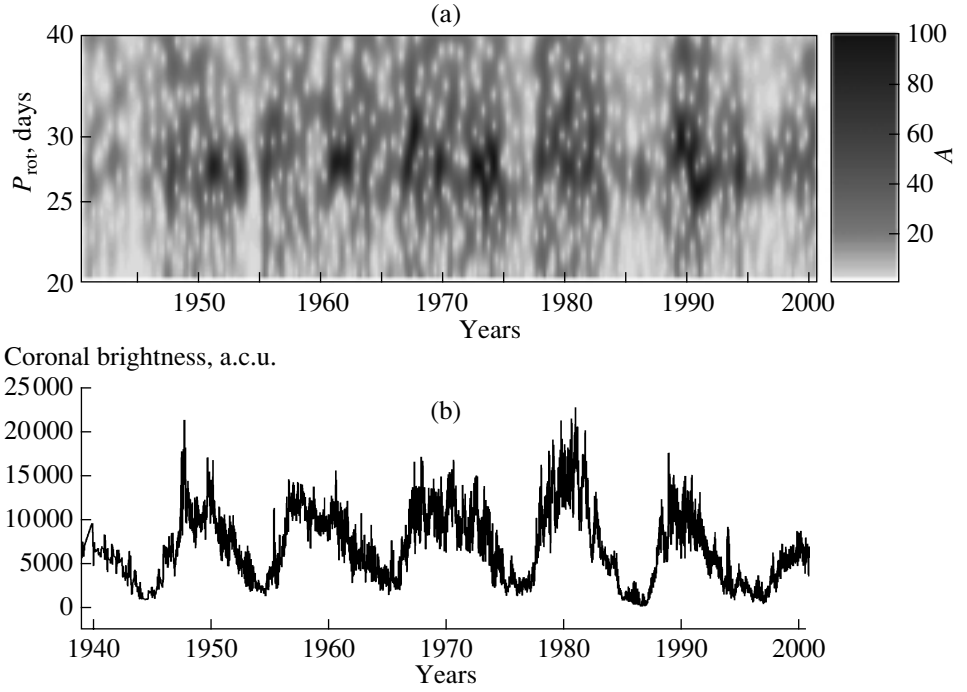

Fig. 2. (a) Wavelet analysis of the time series of the solar coronal green-line emission in the form of the GLSun index. The vertical axis indicates the rotational periods in days. The wavelet amplitudes A are normalized using the scale shown at the right. (b) Time variations of the daily GLSun values during the 17th–22nd solar-activity cycles.

flux. The correlation between the daily GLSun values constructed from the original data averaged over three days and the daily 10.7 cm flux sometimes reaches 0.80. Figure 3 shows this correlation for three months in 1991. The correlation during this and similar periods is in fact higher if we eliminate some high radio fluxes attributed to peculiar sources and/or weak flare activity in large sunspot groups. We can see this in Fig. 3b, where that the lower branch is associated with weak non-stationary phenomena. Note that high correlations are not frequently observed, and are absent when active longitudes are essentially absent from the variability of the radiation emitted from all levels of the outer solar atmosphere.

GLSun is a formal quantity measured above the limb that describes the solar activity using the coronal green-line emission. GLSun describes the total emission of the corona except that from regions screened by the solar disk. This total emission includes both the observed coronal emission above the limb and the emission of coronal regions projected onto the disk. Note that these regions are observed directly in the soft X-ray and radio emission.

GLSun has the same units as the coronal brightness $B(\varphi_n)$, namely, erg/cm^2 s ster. Assuming that the radiation is isotropic and multiplying the GLSun by the area of one cell of the map ($\approx 3 \times 10^{19}\ cm^2$), we obtain the flux πS GLSun. The GLSun values reach 10^4 in periods of high activity, which yields a radiation flux of $\approx 10^{24}$ erg/s. Of course, this is only an estimate, since is based on several assumptions, with two of these being most important.

The first assumption is that the brightness of a point observed above the limb corresponds to a tangential integral along the line of sight from minus infinity to plus infinity. It would seem that the values used for regions on the disk are approximately twice those used for points observed above the limb. However, the observations correspond to an altitude of 60″ above the limb, and do not include the contributions of lower coronal layers to the total line emission. In fact, these two effects compensate each other. Therefore, we expect that GLSun describes the total emission of the corona on the disk and above the limb.

The second assumption is that the emission in the GLSun index from a sphere (the synoptic map) can be reduced to the emission of the disk simply using the product of two cosines. Using higher powers, for example cos^2, does not appreciably change the GLSun values. Generally speaking, the data permit precise calculations of the total coronal emission. In principle, we can replace the synoptic map with the total flux, and the corresponding calculation techniques exist. If we know the intensity of the radiation escaping from a coronal region with coordinates φ and λ, we can calculate the flux of the radiation coming to

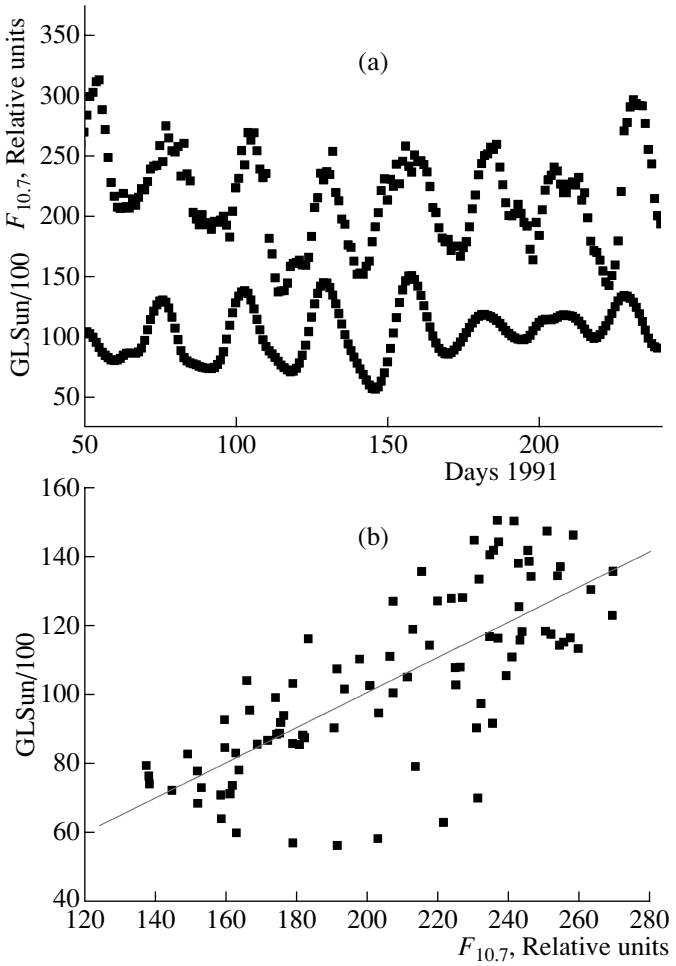

Fig. 3. (a) Variations in GLSun (lower curve) and in the 10.7 cm emission (upper curve) for 1991 (over 91 days). (b) Comparison of these quantities within the same time interval.

the observer. However, there is an important difficulty, namely, we must precisely know the anisotropy of the radiation intensity. The emission of a volume element in the corona is determined by both electron collisions and scattering of the photospheric radiation. The scattering is responsible for the anisotropy of the escaping radiation. The percentage of scattered radiation can be determined from the polarization observed in the line. The polarization can be estimated for limb regions with various activity levels, but significant uncertainties persist in these estimates. A discrepancy between the theoretical and observed positions of the plane of polarization for the radiation in the 5303 Å line [11, 12] aggravates the situation. This unresolved problem leaves the anisotropy of the radiation in the green line unknown.

To verify the total emission presented above, we will estimate the line flux in another way, using eclipse observations. For example, the solar activity was high during the eclipse of July 11, 1991. The GLSun values approached 10^4, and the 10.7 cm radio emission was about 200, approaching the mean level for 1991 (see Fig. 3), which was typical for numerous active periods. During the day of the eclipse, the white corona was almost spherical, and the active longitudes were located near the limb. J. Sykora observed the intensity and polarization of the green line during this eclipse, and his analysis is presented in detail in [13]. Allowing for the absolute calibration used, the total intensity of the corona observed above the lunar edge was about 6×10^{22} erg/s ster. This estimate corresponds to altitudes observed above $1.1 R_\odot$.

We can estimate the emission of the coronal region projected onto the disk using the calculations carried out for the continuum of a hydrostatic isothermal corona presented in [14]. The flux of the line radiation of the isothermal corona is proportional to the volume emission measure. The total emission measure EM of the entire corona (for a solid angle of 4π) takes the form

$$\mathrm{EM} = \mathrm{EM}_{limb} + \mathrm{EM}_{fs} + \mathrm{EM}_{bs},$$

where EM_{limb} corresponds to a source observed at the limb, EM_{fs} to the region projected onto the visible disk, and EM_{bs} to the region shaded by the solar disk (the last two terms are equal for a spherically symmetrical corona). The ratios EM_{fs}/EM from [14] vary from 0.46 to 0.31, depending on the temperature, which lies in the range 1–4.6 MK. Applying these calculations to the line and allowing for the fact that the scattering of the photospheric radiation results in the appearance of some photons at higher altitudes yields about 0.35 for this ratio. In other words, if the green corona was spherically symmetrical on July 11, 1991, the radiation flux from the region projected onto the disk would be very close to that observed at the limb. This flux was overestimated, since the disk activity that day was appreciably lower than the limb activity. Finally, we conclude that the radiation flux emitted from sources on the disk and at the limb on July 11, 1991 reached approximately 10^{23} erg/s ster. This flux corresponds to the emission detected above an altitude of $1.1R_\odot$ and smoothed with the interval of three days. This suggests that the total line emission of the solar corona determined from GLSun is close to the real radiation flux.

Observations of the polarization in the green line enable us to relate GLSun to the emission of the entire solar corona. The intensity of the solar corona can be expressed

$$I_\lambda = I_e + I_{ph},$$

where I_e and I_{ph} are the intensities attributed to excitation of the green line by electron collisions and by the absorption of photospheric photons, respectively. The term corresponding to scattered photospheric radiation becomes significant at fairly high altitudes in the inner corona, as is demonstrated by the changes of the total intensity with altitude. A new method for separating the two components using the anti-correlation between the polarization and intensity of the green line was proposed in the late 1990s [15]. This method was applied to the eclipse of July 11, 1991, when the solar activity was high, yielding the ratio $D = I_{ph}/I_e$ for all points above the limb [13]. During this eclipse, throughout the corona, the flux of scattered radiation did not exceed half the photon flux due to excitation by electron collisions.

Taking this into account, the electron component of the radiation flux emitted by the visible hemisphere (the disk and limb) can be written

$$2/3 \cdot \pi \cdot 3 \times 10^{19}\ \mathrm{GLSun} = \frac{h\nu}{4} a(T) q(\ \mathrm{EM} - \mathrm{EM}_{bs}),$$

where q is the total electron-collision excitation rate for the initial level (taking into account the upper levels) and

$$a(T) \equiv \frac{n(\mathrm{FeXIV})}{n} = \frac{n(\mathrm{Fe})}{n} \frac{n(\mathrm{FeXIV})}{n(\mathrm{Fe})}$$

the relative abundance of the ion Fe XIV. Note that this expression corresponds to an isothermal corona. With $a = 1.05 \times 10^{-5}$ and $q = 10^{-8}$ cm^3 s, we find the total volume emission measure of the active corona $EM - EM_{bs} \approx 6 \times 10^{48}\mathrm{cm}^{-3}$.

Thus, during active periods, the total radiation flux of the entire corona in this forbidden line reaches $\approx 10^{24}$ erg/s, which is lower than the solar soft X-ray luminosity by a factor of 100. For an isothermal corona, GLSun is proportional to the emission of the entire corona, which is appreciably below the emission of the white corona, which approaches the value 3×10^{49} cm^{-3} (1 Baumbah)[14]. Figure 2 shows that the ratios of the maximum and minimum indices are very high for all five cycles. The differences in the minimum values are partially distorted, since the sensitivity of instruments has significantly changed over fifty years, and weaker and weaker brightnesses have been detected. On the other hand, the index remains proportional to the emission of the entire corona only at fairly high activity levels, while the contribution of hot elements of the corona decreases sharply near the activity minima. Since the green line is radiated by hot elements with temperatures of 1.8–2 MK, the total emission decreases sharply at low activity levels. Thus, GLSun describes long-term variations in the emission of hot coronal elements. Other activity indices, such as the 10.7 cm radio emission or the total flux in the H and K CaII lines, which are less sensitive to temperature variations, demonstrate weaker differences between the cycle maxima and minima.

3. WAVELET ANALYSIS OF LONG-TERM VARIATIONS IN THE BRIGHTNESS OF THE CORONA OF THE SUN AS A STAR

Let us examine the daily brightnesses of the corona of the Sun as a star using the same method that is applied to the long-term variability of late-type active stars. We will not use the Fourier transform, which works well for signals that die off at infinity, to identify periodic components in the time series. If, as in our case, the signals do not die off at infinity and the signal may contain oscillations with more or less constant amplitudes, the Fourier integral can diverge. Instead of comparing the signal with sinusoids, as in a Fourier analysis, a wavelet analysis compares the signal with wave trains. In other words, instead of the signal dying off at infinity, the wavelet analysis requires that the comparison function dies off at infinity.

A modified wavelet transform is used in analyses of stellar data, since stellar observations contain large

gaps. The idea of an additive wavelet analysis was proposed in [16, 17] and applied by Katsova et al. [6], who also carried out software tests and comparisons with the Fourier transform. The solar database is free of gaps, since the gaps due to absent observations were filled with interpolated data. Nevertheless, the solar data were analyzed using the same software applied to the stars.

The wavelet transform employs functions with various frequencies and lengths. These functions result from stretching and moving the wave train along the time scale,

$$\psi(t) = e^{-t^2/2} e^{i\omega_0 t}. \quad (1)$$

The wavelet transform is defined by the relations

$$\psi(t', a, t) = \psi\left(\frac{t'-t}{a}\right), \quad (2)$$

$$w(a,t) = C_\psi^{-1/2} a^{-1/2} \int_{-\infty}^{\infty} \psi(t', a, t) f(t') dt'.$$

The adaptive wavelet transform [17] uses the modified wavelet

$$\psi(t', a, t) = e^{-\frac{1}{2}\left(\frac{t'-t}{a}\right)^2} \left(e^{i\omega_0 \frac{t'-t}{a}} - C(a,t)\right), \quad (3)$$

where the coefficient $C(a,t)$ is determined by the normalization of the adaptive wavelet [17].

We carried out our calculations for the stars with three w_0 values, that is, varying the resolution in time and frequency. The final results for the stars and the solar corona are presented for $w_0 = 2\pi \cdot 4$ (i.e., the k used in [17] was 4).

Searches for periods in the stellar data were carried out in the interval from 5 to 100 days, and in the solar data in the interval from 10 to 60 days.

Compared with stellar data, the software processing of the solar data is much more reliable. However, the errors in the rotational periods increase significantly at epochs without coronal observations, i.e., at epochs with interpolated data. This refers mainly to the early observations in 1939–1943, and these years were omitted in our subsequent analysis.

The synodic period of the solar rotation $\langle P_{rot} \rangle = 27.16$ days can be distinguished in both the wavelet amplitudes and, more reliably, the phase of the corresponding changes. Figure 4 presents the power spectrum for all points of the time series (more than 22 500 days). The main peak corresponds to the synodic period, with the spread of 0.034 days. In addition, the power spectrum in Fig. 4 shows a "step" at periods above 30 days that corresponds to the slowly rotating elements observed in some epochs. The formal area of long periods in Fig. 4 is represented by the curve, which encloses an area comparable to that beneath the main maximum. The longer period of 30.95 days is determined with a larger spread of 0.64 days.

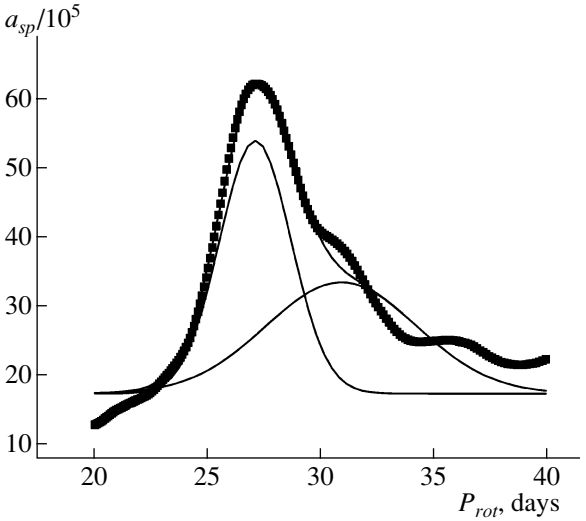

Fig. 4. Analog of the Fourier spectrum of the entire GLSun time series from 1939 to 2001. The vertical axes a_{sp} give the nonnormalized GLSun value per unit frequency corresponding to a period difference of 0.01 days in the range of periods considered. The dependence of a_{sp} on the rotational periods of irregularities P_{rot} is represented by two Gaussian curves.

Figure 2a presents the wavelet transform in period–time coordinates. Here, the wavelet amplitude A is normalized to 100 at its maximum. Comparing the amplitude maxima with the data series itself (Figs. 2a and 2b), we can see that appreciable wavelet amplitudes correspond to epochs of high activity. This indicates some coronal irregularities with slowly varying longitudes. In most cases, these indicate the presence of active longitudes at these epochs.

Of course, Figure 2a also shows the main period of 27 days for the rotation of irregularities. It is important that the rotational periods considerably exceed the mean period $\langle P_{rot} \rangle$ during some epochs with high amplitudes A. Note that the slower rotation appears rapidly and persists over several years; we can see this in the 20th and 22nd cycles. Note also that the lower amplitudes A for the 21st cycle may indicate not only rare active longitudes but a larger spread in the coronal data obtained by various observatories during this period.

The highest wavelet amplitudes appear near the activity maxima. Figure 2a shows regular changes from the maximum period of 30–31 days to the mean period. These changes display different behaviors for different cycles. For example, a single narrow profile

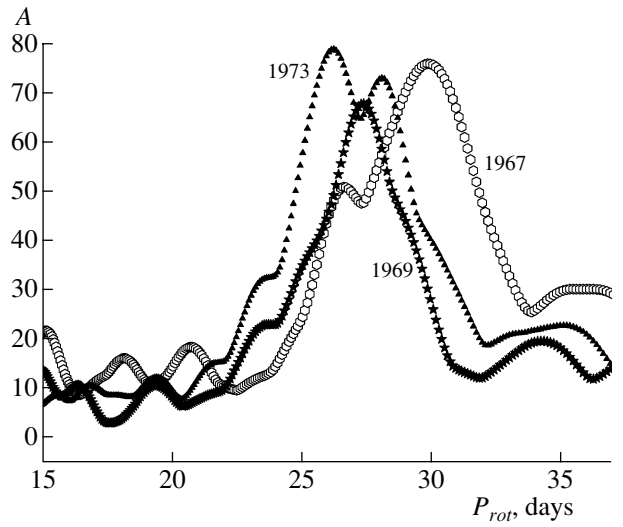

Fig. 5. Period distribution of the wavelet amplitudes A for each of three years near the maximum of the 20th cycle. The time resolution is the same as that in Fig. 4, and the normalization is determined by the length of the series of one year.

was observed in 1991, while, the profile was double-peaked in 1989 and 1990. The corresponding amplitudes reached nearly their maximum possible values, in good agreement with the distinct 27-day changes shown in Fig. 3a. To illustrate gradual changes in the rotational period, we present data related to variations near the synodic periods of 27 days that occurred near the maximum of the 20th cycle (Fig. 5). As a rule, the main peak corresponds to 27 days, while the opposite situation, as occurred in 1967, is rare. However, fast and slow changes occur to some extent in each of the analyzed three years. A general trend from the slow rotation that dominated in 1967 to faster rotation is clearly visible in the 20th and other cycles. It is natural to associate this with the drift of irregularities (or the regions in which they originated) from high latitudes toward the equator, as is typical for sunspots and active regions in general. In the case considered, this behavior is observed when 27-day changes are quite distinct, probably due to the presence of an active longitude. Thus, we expect that this equatorward drift occurs without appreciable changes in longitude. The maximum latitudes of bright coronal elements can be higher than the royal latitudes. It therefore becomes important to examine relationships between the slower rotations of the irregularities and the magnetic fields on various scales.

We can see that slower rotation appears in each cycle. The latitude drift considered can be represented in a form resembling the Maunder diagrams constructed for active regions. The most distinct slower rotation was observed near the maxima of the 20th and 22nd cycles, when periods exhibited by many irregularities exceeded 31 days. This period difference of four days corresponds to a differential rotation rate of $\Delta\Omega/\langle\Omega\rangle = -0.13$. Rotations faster than the mean rotation were revealed for some epochs (about 1973 and 1990).

4. SOLAR ROTATION AND LARGE-SCALE MAGNETIC FIELDS

Since the Sun is by far the nearest star, we can observe various surface irregularities and their motion on the solar surface. These tracers supply us with information on the solar rotation at various levels of the solar atmosphere. To some extent, the rotation of the solar corona displays the same motions as both the active regions at royal latitudes and the large-scale magnetic fields at all latitudes. The results of [18] indicate that the dependences of the rotational characteristics on the magnetic-field strengths at low and high latitudes are different.

Variations in the emission of the Sun as a whole, for example in soft X-rays, in its total emission (the solar constant), etc, also contain information on rotational characteristics. In principle, a spectral–temporal analysis of the observational data can be used to determine the rotational periods exhibited by irregularities. For example, a wavelet analysis of variations in the solar constant was carried out by by Lanza et al. [19], who were able to distinguish irregularities whose rotation was slower than the Carrington rotation during periods of high activity. Since the integrated radiation flux of the Sun is sensitive to sunspots and photospheric faculae, these results correspond only to low latitudes possessing active regions. Stellar chromospheric irregularities are observed both near the equator and at higher latitudes, and we cannot directly compare the results of [6] and [4, 7]. Soft X-ray observations would be preferable for this purpose; however, in addition to the dominating influence of active regions, this tracer is sensitive to numerous weak flares.

We note here the work [20] discussing the evolution of the magnetic moment of the global solar dipolar field. Observations of the large-scale magnetic fields (synoptic maps) and measurements of the magnetic field of the Sun as a star, i.e., the general magnetic field, can be used to determine the characteristics of the magnetic moment and the directions of the dipolar field over the three last solar cycles. Both the magnetic moment and the vertical and horizontal components of the field change in a regular fashion during each cycle, but never disappear completely. When averaged over several rotations, the vertical component smoothly changes, demonstrating a cyclic 10-year variation. The horizontal component manifests itself during periods of high activity

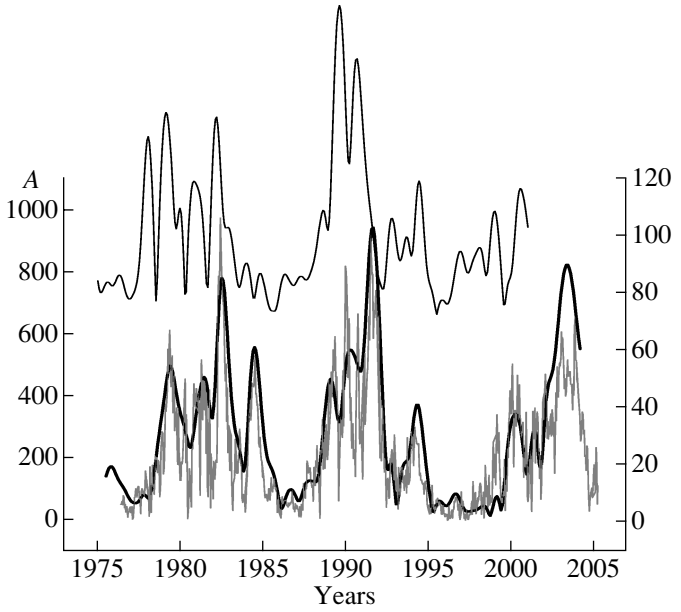

Fig. 6. Wavelet amplitudes of the solar general magnetic field for a period of 27.0 days (bold curve). The lower thin curve shows the horizontal component of the dipolar field in $\mu T/R_\odot^3$; the scale is shown at the right. The upper thin curve presents the wavelet amplitudes for the slower coronal rotation with a period of 30.0 days. The amplitudes A are in arbitrary units, and the zero of the upper curve is shifted to $A = 700$.

near the polarity reversals in each cycle (see Fig. 6). The horizontal component sometimes reaches high strengths compared to the vertical component, and displays a much larger spread. Variations with periods of one to two years probably contribute to these effects. A comparison of the field components with the dipole moment shows that the vertical dipole is observed at cycle minima and the horizontal dipole at maxima. The horizontal dipole is observed during a comparatively short time of about two years. However, before and immediately after the horizontal dipole, there is an inclined magnetic rotator and a strong corrugation in the interplanetary current sheet. In this case, the base of the current sheet that is the neutral line of the large-scale magnetic field reaches high latitudes at some longitudes, as a rule, spreading over 180°.

The wavelet analysis of the general magnetic field (GMF) presented in [20] shows that the amplitude of the 27-day GMF variations is closely related to the magnetic moment of the horizontal dipole. The GMF wavelet amplitude for a period of 27.0 days is closely correlated with the magnetic moment of the horizontal dipole. This is confirmed by a comparison of the two lower curves in Fig. 6, which represent the wavelet transform of the daily magnetic field of the Sun as a star corresponding to a period of 27.0 days [20] and the magnetic moment of the global dipole calculated from maps of the large-scale magnetic field.

This enables us to identify epochs with irregularities displaying slower rotation. Analysis of the long-term variations in the magnetic field of the Sun as a star makes it possible to identify the origin of this effect at a given time. Our wavelet amplitude for the slower rotation with $P_{rot} = 30.0$ days (cf Fig. 2a) is also shown in Fig. 6. We can see that the epochs of slowly rotating elements are near the epochs of the horizontal magnetic dipole of the Sun as a whole.

There is a slight difference between the behavior of the wavelet amplitudes for the coronal index (Fig. 2a) and the solar GMF [20, Fig. 4]. In addition to the main rotational period of the large-scale magnetic field near 27.0 days, there are irregularities that rotate more slowly during epochs of maximum activity. The slowest rotation indicated by the GMF data occurs at the end of the growth phase before the cycle maximum, while the slowest rotation in the corona occurs in the second, coronal, activity maximum. This is also shown in Fig. 6, for example, in the opposite maximum phases for the two lower and upper curves for the high-activity interval of the 21st cycle.

Returning to our findings, we conclude that epochs of slower rotations (see Fig. 2) area near the times of polarity reversals. These epochs are somewhat longer than the polarity reversals in both solar hemispheres, and also encompass the inclined-rotator stage. Large-scale irregularities are observed at latitudes of 40°–50° during these intervals, and it

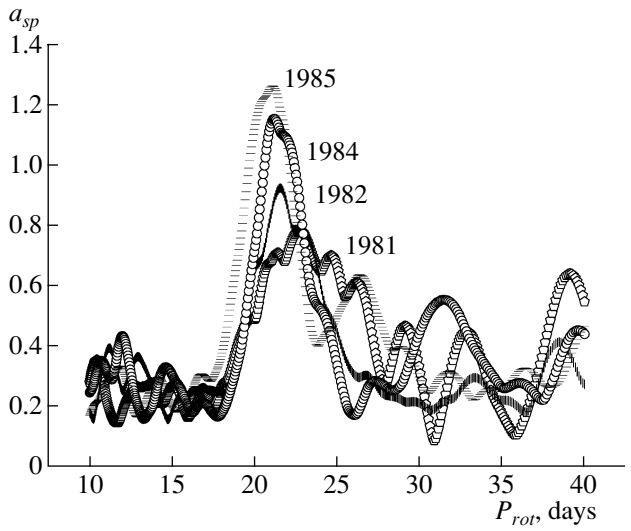

Fig. 7. Wavelet amplitudes for the time series describing the chromospheric emission of HD 149661 during a high-activity period.

is likely precisely these features that are rotating more slowly in this period.

In general, our results support those obtained from the thorough analysis of the coronal rotation in [4], but we note some differences. Our epoch of slower rotation is near the polarity reversal of the global dipole, whereas the epoch of slower rotation in [4] is nearer to the onset of the cycle, and includes the entire growth phase. This difference is mainly due to the fact that the wavelet analysis is not able to include the solar coronal emission during activity minima due to the extremely weak rotational modulation of the signal. On the other hand, our study reveals the role of active longitudes and the magnetic equator during periods of high activity, while these effects are smoothed in analyses for all longitudes within a latitude belt.

5. COMPARISON OF LONG-TERM CHANGES IN THE CORONAL BRIGHTNESSES OF THE SUN AS A STAR AND OF HK STARS

A wavelet analysis of long-term changes in the emission of late-type stars and the Sun proved to be very fruitful. The solar time series contains no large gaps and includes several activity cycles. There is a uniform observational series on long-term variations of the chromospheric emission in the calcium H and K lines for 111 stars in the solar neighborhood (the monitoring started in 1965, in the framework of the HK project). This monitoring has identified more than ten stars with distinct cycles in the chromospheric activity. These stars form the "Excellent" group; about ten other stars demonstrate more irregular cyclicity, and form the "Good" group. The activity of the remaining stars is either irregular or absent.

The first results of a wavelet analysis of the chromospheric emission of twenty HK stars were presented in [6]. All these stars display reliable rotational periods. In addition, the rotational periods of the chromospheric irregularities of some stars vary from year to year. This is most clearly visible for the two "Good" stars HD 149661 and HD 115404, as well as HD 101501, which displays more complex variability. These stars demonstrate a higher activity than do cyclic stars typical for the "Good" group. No appreciable changes in the rotational periods of the "Excellent" stars have been detected.

The wavelet transform of the data series on the solar coronal green line yields results that are essentially the same as those for the chromospheric activity of the "Good" stars. The reliability of the solar analysis is much higher, since the data series is uninterrupted (without gaps) and includes more than five cycles. The main results presented in Fig. 2a essentially confirm the conclusions drawn for HD 115404 and HD 149661, namely, the rotation of surface irregularities is slower in periods of high activity. While the typical variations in the rotational periods (an increase in the period, followed by a gradual return to the mean period and a short interval of more rapid rotation) are only weakly detected in the "Good" stars, these variations are clearly distinguished in the solar rotation, especially during the 20th and 22nd cycles. It is important that the total length of this "wave" can vary from 3 to 4–7 yrs, and is correlated with the length of the period of high activity in the given solar cycle. High wavelet amplitudes appear when the presence of active solar longitudes is revealed by various active elements more or less reliably. If the stellar active longitudes were as pronounced as their solar counterparts, no rotational modulation would be observed, and it would not be possible to study variations in the periods of these stars.

We supplement the results of [6] by analyzing the chromospheric-activity index individually for each year. As an example, Figure 7 presents the wavelet amplitudes for HD 149661 during an epoch of high activity (the duration of its cycle is about 17 yrs, and a cycle of 4 yrs is also detected). The mean rotational period of this star is 21.3 days. We can see that the rotation of irregularities accelerates, and reaches the mean rotation during these years. The difference between the periods is 1.7 days, which corresponds to a differential rotation rate of $\Delta\Omega/\langle\Omega\rangle = (\Omega_{slow} - \langle\Omega\rangle)/\langle\Omega\rangle = -0.074$.

These effects are more distinct for HD 115404. A rotational deceleration of irregularities is revealed near two successive maxima of its 12-year activity cycle. The mean rotational period of this star is

18.5 days; with the period of slower rotation being 21.5 days, the differential rotation rate is −0.14.

These quantities must be compared with the sidereal periods for the Sun. The rotation of the Sun relative to the stars demonstrates a differential rotation rate of −0.16. Consequently, the differential rotation rate of HD 115404 is close to the solar value, while it is half the rate for HD 149661.

Thus, using a single method for the Sun and other stars, we find that the Sun and the "Good" stars demonstrate effects that are similar even in details. The observational conditions for the Sun and the other stars impose some limitations. There are uninterrupted observations for the Sun, as well as additional information on magnetic fields, active elements, etc. In the case of the stars, high-latitude irregularities contribute more strongly to the total emission, probably due to the fact that the inclination of their rotational axes can differ significantly from 90°, making the observational conditions more favorable. We expect that the active longitudes of these stars are more easily detectable than the solar active longitudes. Therefore, the variability in the rotational periods of some stars expressed through long-term variations of their total emission is detected as clearly as in the solar case.

6. DISCUSSION

A wavelet analysis of long-term variations in chromospheric emission of several single stars reveals some year to year changes in their rotational periods that can be associated with probable differential rotation. It is important to compare these conclusions with the available information on the differential rotation of the Sun. Until now, differences in the methods used for analyses for the Sun and other stars have hindered trustworthy comparisons. Here, we first modeled the signal for the total solar coronal emission, then analyzed daily measurements accumulated over more than fifty years using the same method applied to analyze stellar measurements.

The coronal index we have introduced estimates the green line emission both at the limb (similar to eclipse observations) and projected onto the disk. It is important that this estimate requires observations already reduced to a single photometric scale. Taking into account eclipse observations on the intensity and polarization of the emission in the 5303 Å line, we conclude that this data series describes the emission of coronal plasma with temperatures of 1.8–2 MK. The data depend very strongly on the activity, and vary by three–four orders of magnitude from activity maxima to minima.

The wavelet transform used was developed for series with large gaps, and our main goal was to obtain unified information from stellar observations spread over various seasons. At the same time, the reliability of our analysis for the uninterrupted solar data series is very high, and the time resolution is limited only by our three-day averaging of the original daily data. The wavelet amplitudes obtained for the solar corona are very similar to those obtained for several stars with higher and more irregular activity: periods of slower rotation occur during epochs of high activity on both the Sun and these other stars. It is important that this effect is observed during several solar cycles, while it has been observed during only one or two cycles for the other stars.

The differential rotation rates for the stars should be characterized by the ratio $\Delta\Omega/\langle\Omega\rangle$. This rate is half the solar rate for HD 149661 and almost equal to the solar rate for HD 115404. We know the rotational velocity of the equatorial irregularities on the Sun well. Therefore, the rotational frequency as a function of latitude is written in the form $\Delta\Omega/\Omega_{eq} = 1 + \alpha \sin^2 \varphi$.

Note that the equatorial rotational velocity for the Sun is close to the mean velocity. The fastest rotational velocities for the stars are not well known, which impedes analysis of their differential rotation and the construction of butterfly diagrams for the latitude distributions of active regions during various phases of their cycles. Nevertheless, rotational velocities near the mean value are detected on the studied stars for all available observations, including during periods displaying slower rotation. Thus, we conclude that the latitude intervals containing active regions are fairly large for both the Sun and these stars, with the upper boundary of this interval varying during the activity cycle.

It is very important that information on solar magnetic fields on various scales can be used to interpret the stellar data. Slower solar rotation occurs during epochs of polarity reversals, but this effect continues somewhat longer than the polarity reversals near the North and South solar poles. This suggests that the slower rotation originates from large-scale fields that arise when the global dipole approaches its horizontal position, including epochs when the dipole's inclination to the solar rotational axis reaches 60°–90°. Of course, there can be some small-scale elements, but their emergence and subsequent evolution may be determined by the large-scale magnetic field. It is likely that large activity systems or their remnants drifting toward high latitudes contribute to the total emission of the outer layers of the solar and stellar atmospheres.

An important but unsolved problem is why slower rotation of irregularities is not observed for the "Excellent" stars, which display distinct activity cycles and are mainly K stars. Both the wavelet amplitudes and the rotational modulations for these stars are

below those for HD 115404 and HD 149661, and their active longitudes are less pronounced. These amplitudes for the Sun have remained fairly high during the last five cycles. Why does the Sun not display the same behavior as these stars with distinct cycles? We can propose two possible explanations for this.

First, we have analyzed the flux of the coronal but not chromospheric solar radiation, with the contributions of active longitudes and activity systems to the total emission being somewhat different. It would be useful to analyze the emission in the solar CaII H and K lines, but we have no long and uniform data series for such an analysis.

Second, the fifty years of data following the International Geophysical Year demonstrates extremely high solar activity. As part of his study of activity cycles observed during the Maunder minimum, Nagovitsyn [21] has proposed to consider the five powerful maxima of the 19th–23rd solar cycles as a gigantic enhancement of activity. This could result in an increase in the contribution of large activity systems and active longitudes to the total emission. For these same cycles, the GLSun wavelet amplitudes were high, and comparable to those obtained for the studied stars. It is therefore possible that the Sun has not yet reached the asymptotic activity regime typical for most cyclic K stars. This problem requires further detailed studies.

ACKNOWLEDGMENTS

The authors are grateful to O.G. Badalyan and V.V. Bruevich for their assistance. This work was supported by the State Program of Support for Leading Scientific Schools of the Russian Federation (NSh-1685.2008.2 and NSh-4573.2008.2).

REFERENCES

1. J. Schou, H. M. Antia, S. Basu, et al., Astrophys. J. **505**, 390 (1998).
2. J. G. Beck, Solar Phys. **191**, 47 (1999).
3. R. C. Altrock, Solar Phys. **312**, 23 (2003).
4. O. G. Badalyan, V. N. Obridko, and Yu. Sikora, Astron. Zh. **83**, 352 (2006) [Astron. Rep. **50**, 312 (2006)].
5. O. G. Badalyan, V. N. Obridko, and Yu. Sikora, Astron. Zh. **82**, 535 (2005) [Astron. Rep. **49**, 477 (2005)].
6. M. M. Katsova, Vl. V. Bruevich, and M. A. Livshits, Astron. Zh. **84**, 751 (2007) [Astron. Rep. **51**, 675 (2007)].
7. O. G. Badalyan and J. Sykora, Adv. Space. Res. **38**, 906 (2006).
8. M. Rybanský, Bull. Astron. Inst. Czechosl. **26**, 367 (1975).
9. M. Rybanský, V. Rusin, P. Gaspar, and R. C. Altrock, Solar Phys. **152**, 487 (1974).
10. M. Rybanský, ftp://ftp.ngdc.noaa.gov/STP/ SOLAR_DATA/Rybansky
11. O. G. Badalyan, I. L. Beigman, and M. A. Livshits, Astron. Zh. **78**, 373 (2001) [Astron. Rep. **45**, 321 (2001)].
12. O. G. Badalyan, I. L. Beigman, and M. A. Livshits, Adv. Space Res. **29**, 355 (2002).
13. O. G. Badalyan, M. A. Livshits, and Yu. Sikora, Astron. Zh. **74**, 767 (1997) [Astron. Rep. **41**, 682 (1997)].
14. O. G. Badalyan, Astron. Zh. **63**, 762 (1986) [Sov. Astron. **30**, 452 (1986)].
15. O. G. Badalyan, M. A. Livshits, and J. Sykora, Astron. Astrophys. **349**, 295 (1999).
16. P. Frick, A. Grossman, and Ph. Tchamichian, J. Math. Phys. **39**, 4091 (1998).
17. P. Frick, S. L. Baliunas, D. Galyagin, et al., Astrophys. J. **483**, 426 (1997).
18. O. G. Badalyan and V. N. Obridko, Astron. Zh. **81**, 746 (2004) [Astron. Rep. **48**, 678 (2004)].
19. A. F. Lanza, M. Rodono, I. Pagano, et al., Astron. Astrophys. **403**, 1135 (2003).
20. I. M. Livshits and V. N. Obridko, Astron. Zh. **83**, 1031 (2006) [Astron. Rep. **50**, 926 (2006)].
21. Yu. A. Nagovitsin, Pis'ma Astron. Zh. **33**, 216 (2007) [Astron. Lett. **33**, 340 (2007)].

Translated by V. Badin